Nuclear Science and Techniques (2025) 36:9
https://doi.org/10.1007/s41365-024-01577-0

Optical transmittance and pulse shape discrimination of polystyrene/poly(methyl methacrylate)-based plastic scintillators

Yi-Yao Liang[1] · Ying-Du Liu[1] · Pu-Sen Wang[1] · Jie Bao[2] · Xiao-Ping Ouyang[1]

Received: 13 November 2023 / Revised: 5 August 2024 / Accepted: 7 August 2024 / Published online: 19 December 2024

Abstract
Polymethyl methacrylate (PMMA) is an optically transparent thermoplastic with favorable processing conditions. In this study, a series of plastic scintillators are prepared via thermal polymerization, and the impact of PMMA content on their transparency and pulse shape discrimination (PSD) ability is investigated. The fabricated samples, comprising a polystyrene (PS)-PMMA matrix, 30.0 wt% 2,5-diphenyloxazole (PPO), and 0.2 wt% 9,10-diphenylanthracene (DPA), exhibit high transparency with transmissivity ranging from 70.0 to 90.0% (above 415.0 nm) and demonstrate excellent n/γ discrimination capability. Transparency increased with increasing PMMA content across the entire visible light spectrum. However, the PSD performance gradually deteriorated when the aromatic matrix was replaced with PMMA. The scintillator containing 20.0 wt% PMMA demonstrated the best stability concerning PSD properties and relative light yields.

Keywords Neutron detection · Plastic scintillation · Pulse shape discrimination · Polymethyl-methacrylate · Polystyrene

1 Introduction

Detecting fast neutrons is of practical importance in several fields, ranging from homeland security to nuclear physics research [1–3]. Applications include fast neutron counting of nuclear reaction kinetics and border monitoring against the illicit traffic of nuclear materials [4–6]. A crucial requirement for neutron detectors is distinguishing fast neutrons from gamma-ray backgrounds using pulse shape discrimination (PSD) techniques [7–9]. Substantial efforts have been dedicated over the past 70 years toward developing discrimination algorithms [10–12] and PSD-capable inorganic scintillators, such as $Cs_2LaLiBr_6$, $Cs_2LiLaBr_6$ [13, 14], BaF_2 [15], and CsI(Tl) crystals [16–18] to satisfy various specific detection requirements. Organic scintillators are well-known for their excellent PSD capabilities. However, the high manufacturing costs and potential leakage of toxic, corrosive, and flammable substances [19–21] for single-crystal and liquid scintillators limit their usage. In the late 1950s, low-cost, easily fabricated plastic scintillators were first obtained by F. Brooks [22]. However, their inherently poor PSD and instability led to the established opinion that plastics are unsuitable for efficient neutron and γ-ray (n/γ) discrimination. Between 2011 and 2012, Zaitseva et al. [23] demonstrated that the PSD phenomena in plastics were similar to those occurring in mixed organic liquids and crystals by doping with approximately three orders of magnitude higher concentrations of fluorescent compounds. The EJ-299 and its improved EJ-276/EJ-276 G plastics have been commercialized by Eljen Technology [24] and are widely used as large-volume and low-cost neutron detectors.

The typical composition of a PSD plastic scintillator includes a polymer matrix, primary dye, and secondary fluorescent dye. The energy deposited by the incident particles is mainly absorbed by the matrix and then efficiently transferred through primary and secondary emitters (dyes) via a nonradiative energy exchange mechanism [25]. Polystyrene

This work was supported by the National Natural Science Foundation of China (No. 12027813) and the fund of National Innovation Center of Radiation Application of China (Nos. KFZC2020020501, KFZC2021010101).

✉ Ying-Du Liu
liuyingdu@xtu.edu.cn

✉ Jie Bao
baojie_ciae@126.com

[1] School of Materials Science and Engineering, Xiangtan University, Xiangtan 411105, China

[2] Nuclear Data Key Laboratory, China Institute of Atomic Energy, Beijing 102413, China

Table 1 Composition, shore hardness, and light yield of the prepared samples

Samples	PPO (wt%)	DPA (wt%)	Ratio (PMMA: PS)	Shore hardness (HD)	LY (%), 3 months	LY (%), 9 months
Sample 1	30.0	0.2	0.0% (0.0 g: 5.0 g)	55.4	116.7 ± 6.0	110.0 ± 8.0
Sample 2	30.0	0.2	20.0% (1.0 g: 4.0 g)	59.0	180.3 ± 5.0	157.7 ± 9.0
Sample 3	30.0	0.2	40.0% (2.0 g: 3.0 g)	65.4	93.9 ± 7.0	88.7 ± 8.0
Sample 4	30.0	0.2	50.0% (2.5 g: 2.5 g)	73.2	87.9 ± 8.0	84.2 ± 8.0
Sample 5	30.0	0.2	60.0% (3.0 g: 2.0 g)	73.4	91.7 ± 6.0	73.9 ± 7.0
Sample 6	30.0	0.2	80.0% (4.0 g: 1.0 g)	78.2	79.5 ± 5.0	78.4 ± 7.0
Sample 7	30.0	0.2	90.0% (4.5 g: 0.5 g)	86.2	N	N

Amounts of PMMA, PPO, and DPA are represented by the weight percentage (wt%) relative to the total matrix (PS, PMMA). The mechanical hardness was measured using a NscingES LX-D Shore durometer (HD). Light yields for samples after three and nine months of storage were calculated by comparing the maximum positions of ^{137}Cs Compton edges with the control sample EJ-276 in the pulse height spectra (Fig. 6)

(PS) and polyvinyltoluene (PVT) are the most commonly used polymer matrices because of their high amounts of benzene rings, which are beneficial for the light yield and PSD performance of the scintillators. However, they are incompatible with many dye compounds that are necessary for efficient PSD in plastics [26]. Fortunately, polymethyl-methacrylate (PMMA), which is an amorphous polymer, exhibits excellent compatibility and facile processing conditions. It lacks benzene rings in its backbone [25, 27] and does not participate in the excitation or energy transfer processes. The polymer is cost-effective, transparent, harder than PS or PVT, and colorless, with a glass transition temperature range from 100 to 130 °C, and has a density of 1.20 g/cm^3 at room temperature [28]. Therefore, the PMMA is widely used in biomedicine, polymer conductivity, and nanotechnology [29–31]. The addition of PMMA was previously investigated by Martinez et al. [32], who found that the introduction of PMMA at high concentrations did not significantly affect the performance of scintillators doped with fluorescent dyes, as reported in previous studies [32].

This study aims to investigate the influence of PMMA on the optical transmittance and PSD performance of plastic scintillators. Samples were prepared using pure PS and PS-PMMA mixed matrices doped with 30.0 wt% 2,5-diphenyloxazole (PPO) as the primary dye and 0.2 wt% 9,10-diphenylanthracene (DPA) as the secondary dye/wavelength shifter.

2 Experimental methods

PSD plastic scintillators were prepared by bulk polymerization of methyl methacrylate (MMA, >99%) and styrene (>99%) monomers obtained from TCI Development Co., Ltd. (Shanghai). The initiator azodiisobutyronitrile (AIBN, >98%) was purchased from Sigma-Aldrich (China). PPO (99.9%) and DPA (99.9%) were obtained from Energy Chemical (China). The chemical structures of the compounds are shown in Fig. 1. The monomers were purified through an aluminum oxide column to remove inhibitors. To impart PSD capabilities of the scintillators, PPO, DPA, and AIBN with mass fractions of 30.0 wt%, 0.2 wt%, and 0.05 wt%, respectively, were added to the mixed matrix of MMA and styrene monomers. The solution obtained in the glass vials was sonicated for 3–5 min until a uniform, clear solution was obtained and then rapidly frozen in a liquid nitrogen bath before being deoxygenated for 3.0 min. To completely remove any remaining oxygen, the solid mixture was melted into a liquid under Ar gas at room temperature. These freeze-pump-thaw steps were repeated at least three times before the vials containing the solid mixtures were sealed in an oxygen-free atmosphere. The vials were placed in a thermostat and heated to 50.0 °C/h for 48.0 h to promote radical thermal polymerization and prevent the formation of cracks and bubbles. This was followed by heating at a rate of 5.0 °C/h to 110.0 °C/h for 72.0 h. Finally, the vials were cooled at a rate of 5.0 °C/h to 50.0 °C/h for another 48 h and then slowly cooled to room temperature. The samples were carefully removed from the vials after cooling in a thermostat.

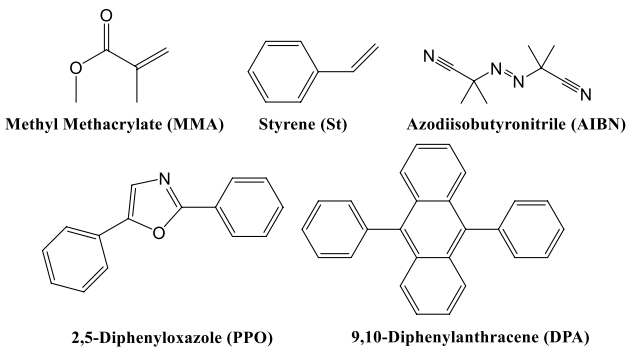

Fig. 1 Chemical structures of the MMA, styrene, AIBN, PPO, and DPA

The nonaromatic matrix PMMA was added in the plastics in increments of 20.0 wt% or 10.0 wt% by following the formulation shown in Table 1. The obtained samples, denoted as Samples 1–7 in the subsequent sections, were machined and polished in advance for performance characterization on both the top and bottom faces using standard polishing procedures. Their sizes, measuring 20.0 mm in diameter and 10.0 mm in thickness, are the same as the control sample EJ-276 used for comparison. The difference in thickness between the samples was measured using a Mitutoyo micrometer (Mitutoyo Corp.) and found to be within 50 µm. The samples were completely colorless and transparent to the naked eye (Fig. 2).

To investigate the effect of PMMA on the mechanical hardness of the monolith, the samples were assessed using a NscingES LX-D Shore durometer. Five equidistant points on the flat side of each sample were measured and averaged to obtain a hardness value with less than 5.0% uncertainty. Photoluminescence (PL) spectra and UV-visible range transmissivity (T%) were determined using an FLS1000 fluorescence spectrofluorimeter (Edinburgh Instruments) and a UV–visible-near-infrared photometer (Lambda750, PerkinElmer Instruments), respectively. To avoid differences in PL intensity that are not correlated to the emission itself, the exciting beam was focused on the front-end surfaces of the solid samples, with the measurement time and conditions maintained at a constant during testing. The PSD capability of the scintillators after 3 months of storage was evaluated by the charge integration method using a ^{252}Cf isotope source (1.0×10^{17}cps/sr) placed $3-4$ cm in front of the samples. To optimize the light collection, the lateral and front sides of the scintillators were wrapped with PTFE tape in several layers, and the opposite sides were coupled to a Hamamatsu photomultiplier tube (PMT, H1949-51) with optical dimethyl silicone (Dow Corning, PMX-200). The PMT was shielded using 5.0 cm-thick lead bricks and biased to the optimized value of −1200.0 V using a high-voltage power supply CAEN N1470. The data were acquired using a CAEN DT5730 14-bit digitizer operating at 500MS/s. DPP-PSD firmware and CAEN CoMPASS software (Viareggio, Italy) were used to obtain the waveforms. The CoMPASS software allows online/offline long- and short-waveform integration, time-stamp recording, and pulse shape discrimination. To ensure uniformity among the samples, consistent test conditions were maintained throughout the measurements.

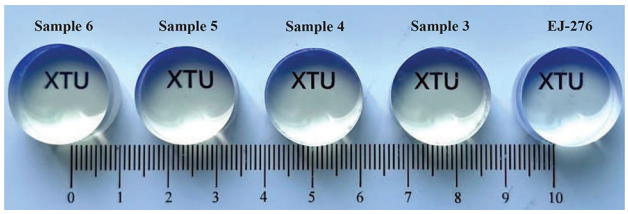

Fig. 2 (Color online) Freshly prepared PS-PMMA-based plastic scintillators with a measured size of ϕ20 mm × 10 mm. From left to right are Samples 6 to 3 containing 80.0, 60.0, 50.0, and 40.0 wt%, respectively, of PMMA in the total matrix, and 30.0 wt% PPO and 0.2 wt% of DPA

The principle behind PSD scintillators discriminating between neutrons and gamma rays is based on pulse shape differences. When neutrons (gamma rays) interact with a scintillator, the resulting scintillation waveform comprises fast (∼ few ns) and slow (delayed) components. The fast component arises from the direct radiative de-excitation of the singlet states (S_1) to the ground states (S_0). In contrast, the slow component over a longer timescale (∼ hundred ns) arises from the bimolecular process of triplet–triplet annihilation (TTA, $T_1 + T_1 \rightarrow S_1 + S_0$). The pulse shape difference between the neutrons and gamma rays mainly originates from the slow component. With the dependence of the triplet state density on the ionizing power of incoming particles, recoiling protons generated by neutron elastic scattering yield a higher number of triplet states and, thus, a pronounced slow component compared to those caused by the electrons from gamma rays. By integrating over both a short-time gate (Q_{short}, mainly a fast component) and a long-time gate (Q_{total}), a particle size distribution factor can be defined as $PSD = 1 - Q_{\text{short}}/Q_{\text{total}}$, where Q_{short} and Q_{total} are the integrations from the beginning of a waveform to its nearby peak and the entire integration, respectively. In the 2D plots of PSD versus Q_{total}, a clear separation of neutrons from gamma rays can be observed, where the locus for larger PSD values is attributed to neutron events and the locus for smaller PSD values is attributed to gamma rays. To quantitatively evaluate the samples n/γ PSD capability, a figure of merit (FoM) is defined as $FoM = S/(w_{\text{n}} + w_{\gamma})$, where S is the separation between the neutron and gamma peaks in the 1D PSD distribution, w_{n} and w_{γ} are the full width at half maximum (FWHM). By adjusting the length of the time gates, the PSD factor can be altered to achieve good separation of incident particles [21]. Optimal PSD values were obtained during the measurements using a 50.0 ns short gate and 450.0 ns long gate. For the measurements of the 3-month storage samples, no electron-equivalent energy calibration was performed for any of the samples, resulting in arbitrary units for Q_{total} in the PSD spectra. Unfortunately, Sample 7 encountered accidental damage during handling; therefore, measurements of its properties were not performed.

The samples were stored in an unsealed drying oven, which inevitably caused slight coloration and degradation of the light output over time. After an additional 6 months of storage, n/γ PSD measurements were performed again with the PMT biased at a higher voltage of −1600.0 V owing to material aging. Calibration of the samples' electron-equivalent energy (unit: keVee) was performed using ^{137}Cs, ^{60}Co, and ^{40}KCl salt gamma-ray sources. The relative light yield

was calculated by comparing the light output with that of EJ-276 through Gaussian fitting to the maximum position of ^{137}Cs Compton edge (480 keVee).

3 Results and discussion

PS is a simple polymer containing a single aromatic ring in each repeating unit and emits UV light with a 310.0-nm emission maximum. The interaction between the aromatic rings of the phenyl groups results in absorption in the range of 200.0–320.0 nm with a peak at approximately 290.0 nm [33]. As previously stated, the introduction of PMMA afforded harder plastics for cutting and polishing with a 7–55% enhancement in mechanical hardness (see Table 1). Still, it did not alter the plastic fluorescence emission spectrum owing to its nonaromatic nature. Figure 3 shows the emission spectrum excited at 310.0 nm by an FLS1000 fluorescence spectrofluorometer. For all samples with dopants of 30.0 wt% PPO and 0.2 wt% DPA, the emission peaks at approximately 365.0 nm for PPO characteristic emission [26] and 412.0 nm, 432.0 nm for DPA dye are observed. The PPO dye molecules absorbed at 300.0−340.0 nm and emitted over the range of 340.0−420.0 nm. By the PPO-DPA dye pair wavelength shifting, the obtained plastic system mainly emitted the blue light required for device photon-electric conversion.

There were many conjugated structures in the benzene rings of the PS matrix. The π bond contained in these structures is beneficial for the exciton migration induced by incident particles. The replacement of the PS matrix with a nonaromatic PMMA matrix degrades the light output. However, the fluorescence intensity of the PS-PMMA plastic at 310.0-nm ultraviolet excitation increased as PMMA concentration increased (Fig. 3), contrary to the expectations. This may be explained as follows: increasing the percentage of PMMA leads to an increase in transparency or a decrease in fluorescence reabsorption, and more PPO dye molecules in excessive amounts participate in direct excitation. Direct excitation is beneficial for scintillation generation up to a specific limit; however, the further addition of PMMA is detrimental. As PMMA increased up to approximately 90.0 wt%, the amount of PS matrix useful for scintillation via energy transfer to primary and secondary dyes was significantly low, and a noticeably reduced fluorescence intensity over the visible light range was expectedly observed, as shown in Fig. 3. Moreover, the dissolution of PPO in PMMA was not as favorable as that in PS; hence, the formation of aggregates and scattering centers was most likely to occur at low PS amounts (Fig. 4). This negatively affects the fluorescence collection through the loss of transmittance along the path of the photons passing through the scintillator. The dependence of the transmittance on PMMA is shown in Fig. 5. The samples exhibited strong absorption in the range of 200.0 − 415.0 nm wavelength. They were optically transparent above 415.0 nm with a high transmissivity of 70.0% ~ 90.0%, and all behaved better than pure PS or PVT-based EJ-276 plastic scintillator. With an increase in PMMA, the transmittance tends to increase over the entire visible light range. However, it decreased as the concentration of PMMA

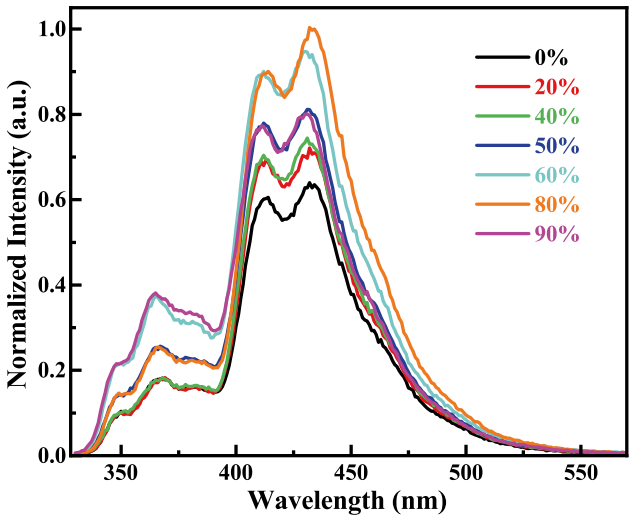

Fig. 3 (Color online) Comparison of fluorescence intensity for the prepared samples doped with 30.0 wt% PPO, 0.2 wt% DPA, and PMMA in different concentrations (0−90.0 wt%). The samples were excited with a 310.0 nm-wavelength UV light

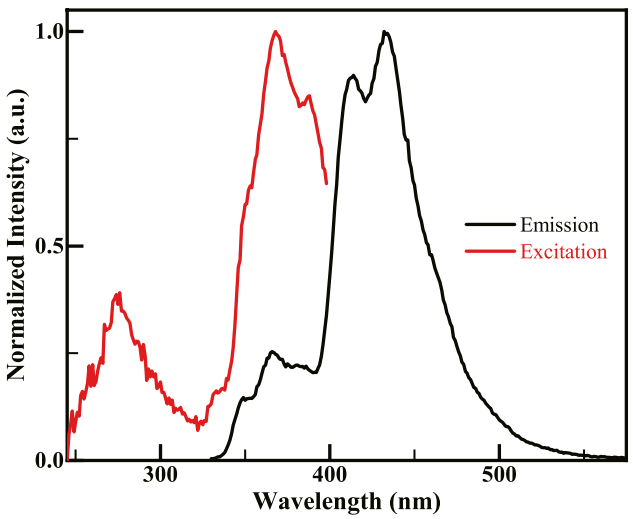

Fig. 4 (Color online) Excitation-emission spectra of Sample 6. The excitation spectrum with excitation wavelengths of 0 − 390.0 nm was recorded at the 433.0 nm emission maximum, whereas the fluorescence emission spectra were induced by a 310.0 nm-wavelength UV

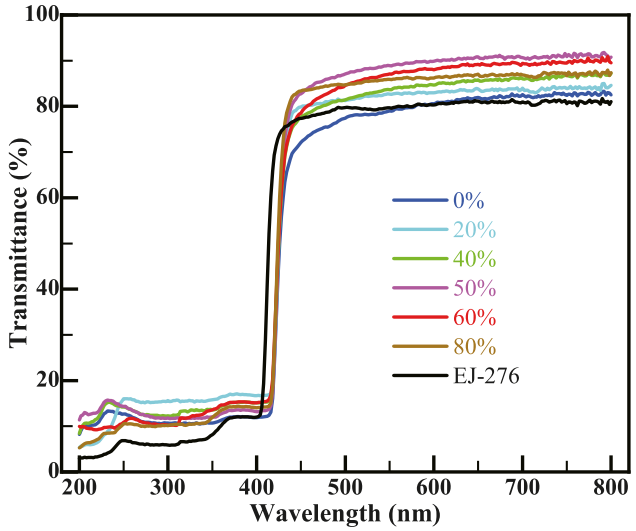

Fig. 5 (Color online) Transmittance of EJ-276 and the prepared samples with PMMA at concentrations of 0–80 wt%

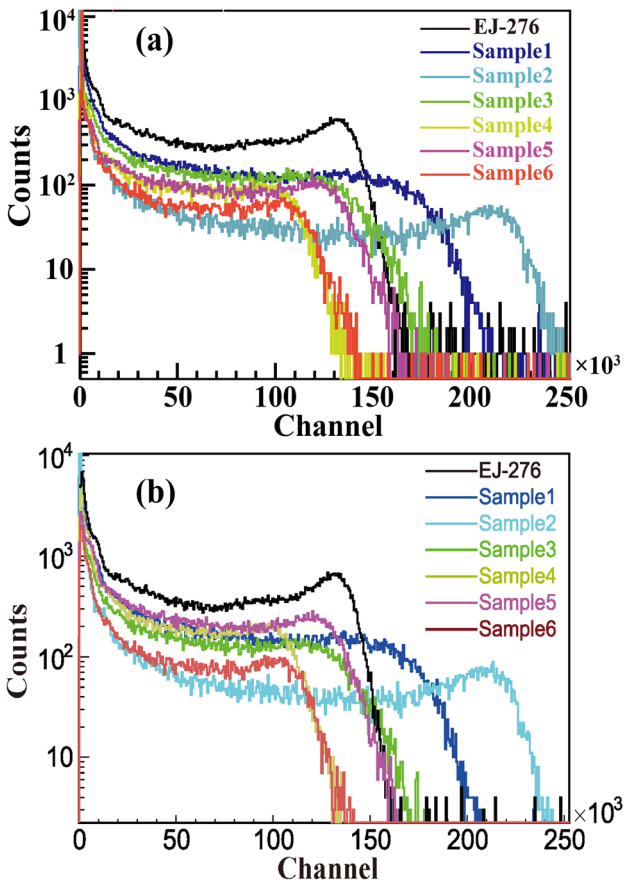

Fig. 6 (Color online) Pulse height spectra of the control sample EJ-276, and Samples 1–6 after three months and nine months storage, measured under the ^{137}Cs source

increased above 50.0 wt%, possibly because of Rayleigh scattering of the aforementioned dye aggregation.

A high light yield (LY), which is predominantly determined by singlet S_1 energy transfer within the scintillator, is always desirable. An enhanced LO can lead to an increase in the PSD FoMs [34]. The effect of PMMA on LY was assessed by measuring the pulse height spectra of the samples after 3 and 9 months of storage using a ^{137}Cs source (Fig. 6a, b). The percentages of the evaluated LO relative to EJ-276, determined through Gaussian fitting to the maximum positions of the Compton edges, are presented in the final two columns of Table 1. The relative LY remained generally stable when comparing the two measurements for each sample, and it showed an overall decrease with the addition of PMMA. This indicates that the scintillators' light output was compromised by the incorporation of the nonaromatic PMMA matrix. Sample 2 containing 20.0 wt% PMMA exhibited the highest relative LO intensity. Because the measured LO is related to the optical interface (including flatness and optical coupling) between the PMT and scintillator, the potential effect on the surface morphology caused by the presence of the PMMA matrix should be investigated in the future.

To understand how PMMA affects PSD performance, samples of 3-month storage were investigated using the ^{252}Cf source. The 2D distributions and obtained FoM values of the PSD are shown in Figs. 7 and 8 (black points). Both the neutron-gamma separation and FoM values decreased gradually with increasing PMMA concentration. According to a commonly accepted mechanism [34, 35], the separation between neutrons and gamma rays in a 2D PSD distribution mainly depends on the probability of the TTA process [34] which gives rise to the PSD phenomenon. To promote the TTA process, both an aromatic matrix and a certain dye load are required to provide high numbers of π electrons and physical proximity of interacting T_1 state molecules [23, 36, 37]. When the aromatic PS matrix is gradually replaced by the nonaromatic PMMA matrix in 20.0 or 10.0 wt% increments, the number of T_1 states transferred nonradiatively from PS to dye molecules [38] is reduced. Consequently, the PMMA matrix decreased the TTA bimolecular process and even the FoM value (Fig. 7). After nine months of storage, the PSD values of the samples and EJ-276 varied quadratically with Q_{total} (Figs. 9, 10). The corresponding FoM values evaluated over the energy range of 200.0 keVee to 800.0 keVee (Fig. 8 (red points)) decreased and fluctuated with increasing PMMA concentrations. Although the two PSD measurements cannot be directly compared because of the different voltages supplied to the PMT, it can be deduced that the addition of PMMA makes the PSD stability complex. PMMA has significantly high chain stiffness and rigidity [39], and its incorporation into the PS matrix improves the mechanical hardness and possibly the physical stability of the samples; however, the generated residue stress that is sensitive to the PMMA amount would lead to

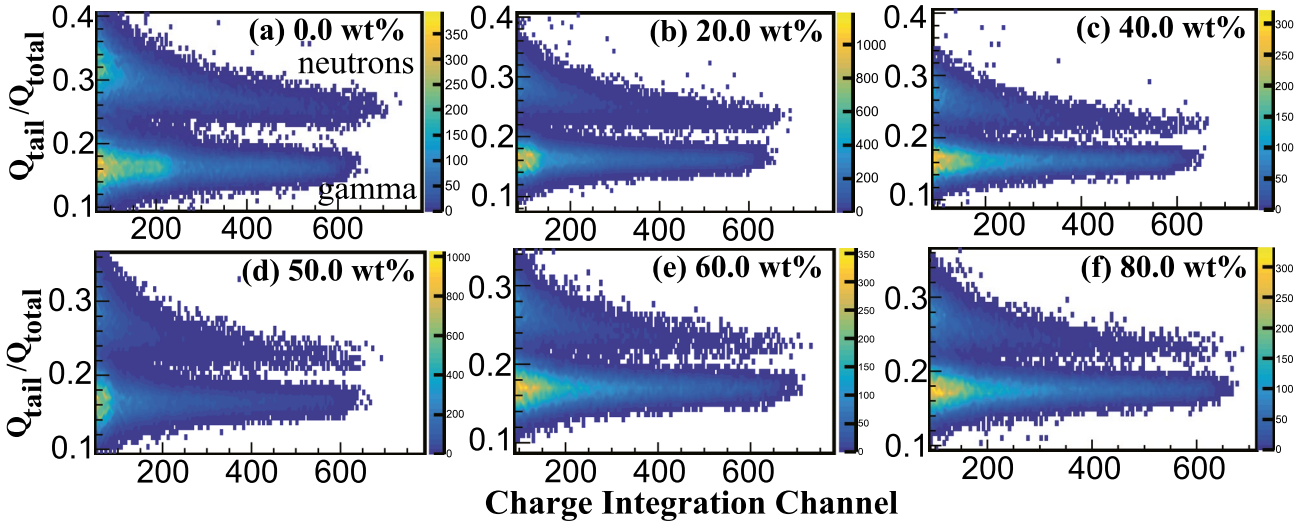

Fig. 7 (Color online) 2D distributions of PSD vs Q_{total} for the samples after three-month storage at air condition, with PMMA at (a) 0.0 wt% (Sample 1), (b) 20.0 wt% (Sample 2), (c) 40.0 wt% (Sample 3), (d) 50.0 wt% (Sample 4), (d) 60.0 wt% (Sample 5), and (f) 80.0 wt% PMMA (Sample 6), respectively. The samples were radiated with the ^{252}Cf source

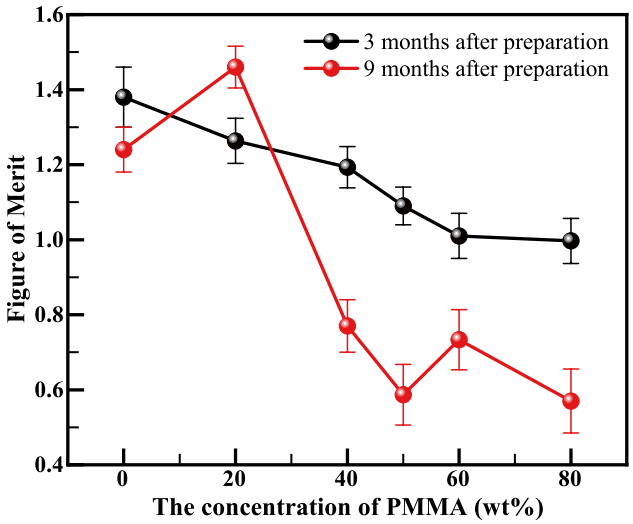

Fig. 8 (Color online) FoM values of the samples after 3 months storage at air condition (black points) and after 9 months storage (red points), as a function of PMMA concentration. The values for the two times measurements were calculated over a Q_{total} channel range of 0.0 to 600.0 (a.u.) and over an equivalent electron energy range of 200.0 keVee to 800.0 keVee, respectively. The solid lines are used only for eye guidance

changes in both the physical morphology and PSD capability over a long timescale. From this viewpoint, the abnormally high FoM value of Sample 2 in the second measurement may imply an appropriate PMMA content.

4 Summary

Plastic scintillators based on PS or PVT matrices are capable of detecting neutrons and gamma rays. To understand the role of PMMA in the transparency and PSD properties, we synthesized a series of plastic scintillators containing a PS-PMMA copolymer matrix doped with 30.0 wt% PPO and 0.2 wt% DPA dye molecules. The measurement results suggest that PMMA degrades the PSD performance and reduces the light yield. However, replacing the PS matrix with non-aromatic PMMA significantly increases transparency and allows the dye molecules to participate in direct excitation. As a result, the fluorescence intensity increased with increasing PMMA concentration. The variation in the stability of the mixed-phase morphology and exciton migration network of the PS-PMMA copolymer may also be attributed to the PMMA amounts. Despite the deterioration of the n/γ discrimination capability, the incorporation of PMMA offers

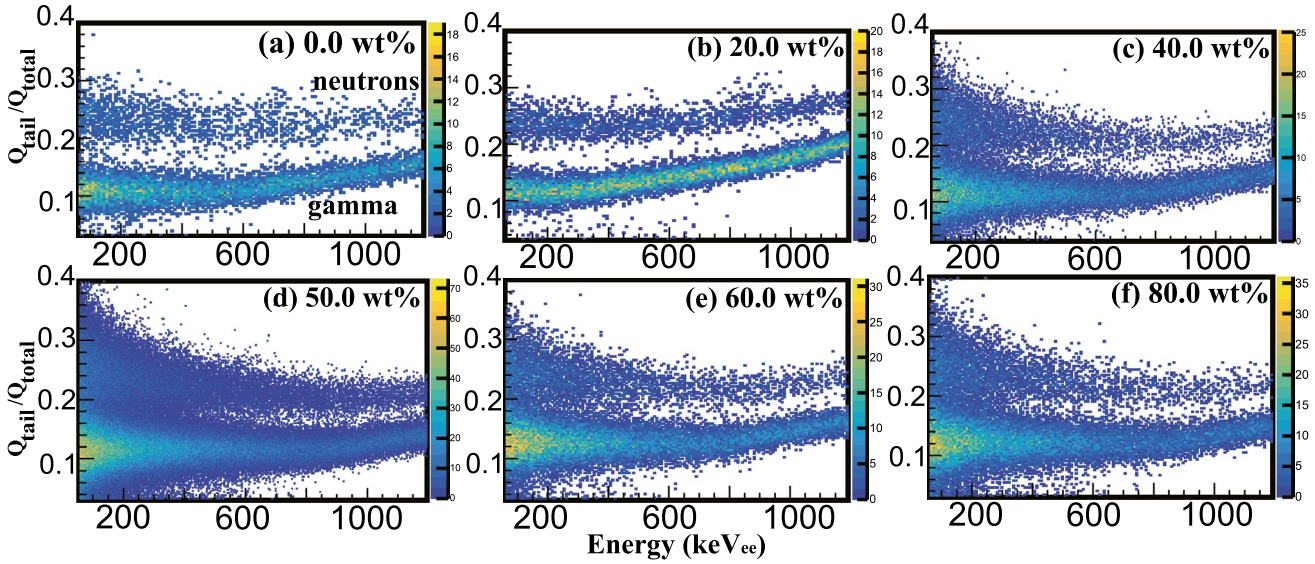

Fig. 9 (Color online) 2D distributions of PSD versus Q_{total} (Energy/keVee) for Samples 1–6 after 9-month storage at air conditions

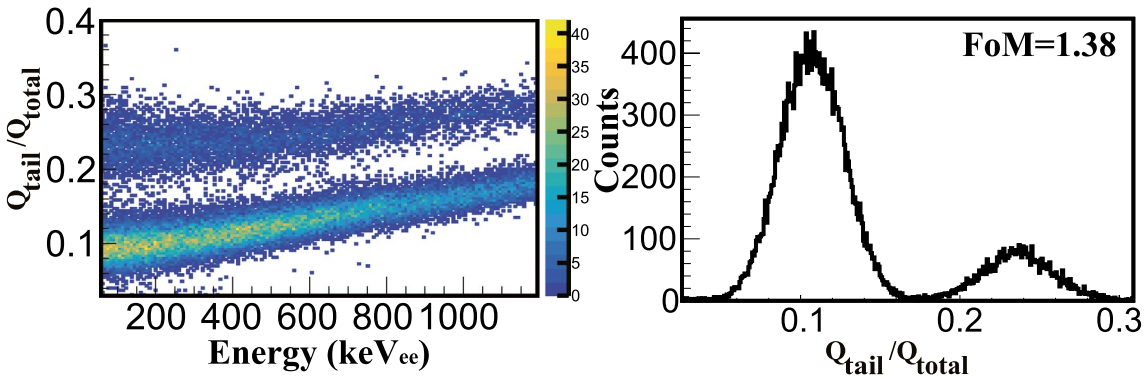

Fig. 10 (Color online) 2D distribution of PSD vs Q_{total} (Energy/keVee) for the control sample EJ-276 (left) and the corresponding 1D distribution. The FoM value was 1.38 in the equivalent electron energy range of 200.0 keVee to 800.0 keVee (right)

superior transmittance and significant mechanical hardness enhancement, making it attractive for the development of physically stable and chemically available compounds for manufacturing PSD-capable scintillators.

Author Contributions All authors contributed to the study conception and design. Material preparation, data collection and analysis were performed by Yi-Yao Liang, Pu-Sen Wang, Jie Bao, and Ying-Du Liu. The first draft of the manuscript was written by Yi-Yao Liang and all authors commented on previous versions of the manuscript. All authors read and approved the final manuscript.

Data availability The data that support the findings of this study are openly available in Science Data Bank at https://cstr.cn/31253.11.sciencedb.j00186.00303 and https://www.doi.org/10.57760/sciencedb.j00186.00303.

Declarations

Conflict of interest The authors declare that they have no Conflict of interest.

References

1. K.J. Chen, L.X. Liu, Z.R. Hao et al., Simulation and test of the SLEGS TOF spectrometer at SSRF. Nucl. Sci. Tech. **34**, 47 (2023). https://doi.org/10.1007/s41365-023-01194-3
2. E. Aboud, S. Ahn, G.V. Rogachev et al., Modular next generation fast neutron detector for portal monitoring. Nucl. Sci. Tech. **33**, 13 (2022). https://doi.org/10.1007/s41365-022-00990-7
3. X.F. Jiang, J.R. Zhou, H. Luo et al., A large area ^{3}He tube array detector with vacuum operation capacity for the SANS instrument at the CSNS. Nucl. Sci. Tech. **33**, 89 (2022). https://doi.org/10.1007/s41365-022-01067-1

4. S. Li, X. Ai, Z. Yu et al., Development of a radiation monitoring system in aviation security check with plastic scintillation detectors and He-3 gas proportional tube detectors. J. Radioanal. Nucl. Chem. **332**, 2581–2588 (2023). https://doi.org/10.1007/s10967-023-08939-9
5. K. Li, J.R. Zhou, X.-D. Wang et al., Study of a nTHGEM-based thermal neutron detector. Chin. Phys. C **40**, 076002 (2016). https://doi.org/10.1088/1674-1137/40/7/076002
6. D.J. Zhao, S. Feng, P.J. Cheng et al., Conceptual design of a $Cs_2LiLaBr_6$ scintillator-based neutron total cross section spectrometer on the back-n beam line at CSNS. Nucl. Sci. Tech. **34**, 3 (2023). https://doi.org/10.1007/s41365-022-01152-5
7. M.L. Roush, M.A. Wilson, W.F. Hornyak, Pulse shape discrimination. Nucl. Instrum. Meth. **31**(1), 112–124 (1964). https://doi.org/10.1016/0029-554X(64)90333-7
8. X.L. Luo, Y.K. Wang, J. Yang et al., Neutron/gamma discrimination employing the power spectrum analysis of the signal from the liquid scintillator BC501A. Nucl. Instrum. Meth. Phys. A **717**, 44–50 (2013). https://doi.org/10.1016/j.nima.2013.04.004
9. Y.H. Chen, X.M. Chen, X.D. Zhang et al., Study of n-γ discrimination in low energy range (above 40 keVee) by charge comparison method with a BC501A liquid scintillation detector. Chin. Phys. C **38**, 036001 (2014). https://doi.org/10.1088/1674-1137/38/3/036001
10. G. Yuan, J. Chen, Q. Yang et al., A digital delay-line-shaping method for pulse shape discrimination in stilbene neutron detector and application to fusion neutron measurement at HL-2A tokamak. Nucl. Instrum. Meth. Phys. A **687**, 7–13 (2012). https://doi.org/10.1016/j.nima.2012.05.077
11. L. Chang, B.Q. Liu, Y.C. Yan et al., Anti-noise performance of the pulse coupled neural network applied in discrimination of neutron and gamma-ray. Nucl. Sci. Tech. **33**, 75 (2022). https://doi.org/10.1007/s41365-022-01054-6
12. L. Chen, X. Xu, G. Jin et al., Fast FPGA algorithm for neutron-gamma discrimination. Nucl. Instrum. Meth. Phys. A **1027**, 166256 (2022). https://doi.org/10.1016/j.nima.2021.166256
13. K. Wu, H. Zhu, L. Zhang et al., Improved discrimination performance of $Cs_2LaLiBr_6$ single crystal detector with doping Y Nucl. Instrum. Meth. Phys. A **1051**, 168188 (2023). https://doi.org/10.1016/j.nima.2023.168188
14. S.X. Liu, W. Zhang, Z.H. Zhang, Performance of real-time neutron/gamma discrimination methods. Nucl. Sci. Tech. **34**(1), 8 (2023). https://doi.org/10.1007/s41365-022-01160-5
15. C.F. Yang, C.Q. Feng, S.B. Liu et al., FPGA-based α/γ pulse shape discrimination for BaF_2 detector using 2 Gsps fast waveform sampling. Nucl. Sci. Tech. **28**, 19 (2017). https://doi.org/10.1007/s41365-016-0173-8
16. J.Q. Faisan, J. Lou, Z. Li et al., A pulse shape discrimination of CsI(Tl) crystal with ^{6}He beam. Nucl. Sci. Tech. **21**, 35–38 (2010). https://doi.org/10.13538/j.1001-8042/nst.21.35-38
17. H.Y. Zhu, J.L. Lou, Y.-L. Ye et al., Two annular CsI (Tl) detector arrays for the charged particle telescopes. Nucl. Sci. Tech. **34**, 159 (2023). https://doi.org/10.1007/s41365-023-01319-8
18. K. Sun, G. Zhang, H. Yi et al., The light charged particle detector array at the CSNS Back-n white neutron source. J. Instrum. **18**, P04004 (2023). https://doi.org/10.1088/1748-0221/18/04/P04004
19. C. Aberle, J.J. Li, S. Weiss et al., Optical properties of quantum-dot-doped liquid scintillators. J. Instrum. **8**, P10015 (2013). https://doi.org/10.1088/1748-0221/8/10/p10015
20. M. Yeh, S. Hans, W. Beriguete et al., A new water-based liquid scintillator and potential applications. Nucl. Instrum. Meth. Phys. A **660**(1), 51–56 (2011). https://doi.org/10.1016/j.nima.2011.08.040
21. O. McCormack, L. Giacomelli, G. Croci et al., Characterization and operational stability of EJ276 plastic scintillator-based detector for neutron spectroscopy. J. Instrum. **16**(10), P10002 (2021). https://doi.org/10.1088/1748-0221/16/10/p10002
22. F. Brooks, Pulse shape discrimination in a plastic scintillator. IEEE Trans. Nucl. Sci. **7**(2–3), 35–38 (1960). https://doi.org/10.1109/TNS2.1960.4315733
23. N. Zaitseva, B.L. Rupert, I. Pawelczak et al., Plastic scintillators with efficient neutron/gamma pulse shape discrimination. Nucl. Instrum. Meth. Phys. A **668**, 88–93 (2012). https://doi.org/10.1016/j.nima.2011.11.071
24. Eljen Technology, Pulse shape discrimination EJ-276D and EJ-276G. Eljen Technology Company website. https://eljentechnology.com/products/plastic-scintillators/ej-276
25. G.H.V. Bertrand, M. Hamel, F. Sguerra, Current status on plastic scintillators modifications. Chem. A Eur. J. **20**(48), 15660–15685 (2014). https://doi.org/10.1002/chem.201404093
26. N.P. Zaitseva, A.M. Glenn, A.N. Mabe et al., Recent developments in plastic scintillators with pulse shape discrimination. Nucl. Instrum. Meth. Phys. A **889**, 97–104 (2018). https://doi.org/10.1016/j.nima.2018.01.093
27. V.N. Salimgareeva, S.V. Kolesov, Plastic scintillators based on polymethyl methacrylate: a review. Instrum. Exp. Tech. **48**, 273–282 (2005). https://doi.org/10.1007/s10786-005-0052-8
28. U. Ali, K.J.B.A. Karim, N.A. Buang, A review of the properties and applications of poly (methyl methacrylate)(PMMA). Pol. Rev. **55**(4), 678–705 (2015). https://doi.org/10.1080/15583724.2015.1031377
29. D. Yuan, W. Zhao, J. Liang et al., Research progress of poly (methyl methacrylate) microspheres: preparation, functionalization and application. Eur. Pol. J. **175**, 111379 (2022). https://doi.org/10.1016/j.eurpolymj.2022.111379
30. Z. Wang, R. Fu, F. Li et al., One-tep polymeric melt encapsulation method to prepare CsPbBr 3 perovskite quantum dots/polymethyl methacrylate composite with high performance. Adv. Funct. Mater. **31**(22), 2010009 (2021). https://doi.org/10.1002/adfm.202010009
31. Y. Hu, S. Zhou, L. Wu, Surface mechanical properties of transparent poly(methyl methacrylate)/zirconia nanocomposites prepared by in situ bulk polymerization. Polymer **50**(15), 3609–3616 (2009). https://doi.org/10.1016/j.polymer.2009.03.028
32. H.P. Martinez, I. Pawelczak, A.M. Glenn et al., Pulse shape discrimination in non-aromatic plastics. Nucl. Instrum. Meth. Phys. A **771**, 28–31 (2015). https://doi.org/10.1016/j.nima.2014.10.023
33. M. Jiang, T. Li, Chunlin Zhou, UV absorption spectra of polystyrene. Pol. Bull. **25**(2), 211–216 (1991). https://doi.org/10.1007/BF00310794
34. N.P. Zaitseva, A.M. Glenn, M.L. Carman et al., Multiple dye interactions in plastic scintillators: Effects on pulse shape discrimination. Nucl. Instrum. Meth. Phys. A **978**, 164455 (2020). https://doi.org/10.1016/j.nima.2020.164455
35. T. Jiang, P.Z. Lu, G. Luo et al., Study on pulse shape discrimination power of plastic scintillator. J. Instrum. **17**(05), T05002 (2022). https://doi.org/10.1088/1748-0221/17/05/T05002
36. L.E. Brady, Handbook of fluorescence spectra of aromatic molecules. J. Medi. Chem. **9**(6), 984 (1966). https://doi.org/10.1021/jm00324a069
37. T. Förster, Mechanisms of Energy Transfer. Compreh. Biochem. **22**, 61–80 (1967). https://doi.org/10.1016/B978-1-4831-9712-8.50010-2
38. G.H.V. Bertrand, M. Hamel, S. Normand et al., Pulse shape discrimination between (fast or thermal) neutrons and gamma rays with plastic scintillators: state of the art. Nucl. Instrum. Meth. Phys. A **776**, 114–128 (2015). https://doi.org/10.1016/j.nima.2014.12.024
39. R. Chakrabarti, D. Chakraborty, Studies on engineering properties of PVC-PMMA semi-interpenetrating polymer networks.

Appl. Pol. Sci. **97**, 1725–1735 (2005). https://doi.org/10.1002/app.21881